Catalysis Science & Technology

ROYAL SOCIETY OF CHEMISTRY

COMMUNICATION

View Article Online
View Journal | View Issue

Cite this: *Catal. Sci. Technol.*, 2020, **10**, 1597

Received 23rd January 2020,
Accepted 14th February 2020

DOI: 10.1039/d0cy00146e

rsc.li/catalysis

Reductant composition influences the coordination of atomically dispersed Rh on anatase TiO_2†

Chithra Asokan, ‡[a] Ho Viet Thang, ‡[bc] Gianfranco Pacchioni *[b] and Phillip Christopher *[a]

Atomically dispersed noble metal catalysts have received recent interest, although the coordination of the metal to the support and how this is influenced by pre-treatment have not often been elucidated. We combine CO FTIR-TPD and DFT to distinguish how catalyst reduction *via* CO or H_2 influence the local metal coordination and molecular desorption processes.

Identifying "the" active site on heterogeneous oxide supported metal catalysts is challenging because metal clusters present sites with varying local coordination environments including metal terraces, steps and metal–support interfaces.[1] Elucidation of active site structures is further complicated by reconstruction, or coverage effects.[1,2] Single late-transition metals atoms (or ions) on oxide supports, sometimes called atomically dispersed metal or single atom catalysts, could enable precise structure–function relationships. However, understanding the catalytic properties of atomically dispersed metals is convoluted by the inherent heterogeneity of the support, where the metal can adsorb at cation vacancies, anion vacancies, on stoichiometric surfaces, on oxidized surfaces and near hydroxyls with distinct characteristics.[3,4] Further, the preferred adsorption geometry may vary as a function of metal loading or environmental conditions.[5–7] Thus, developing structure–function relationships for this class of catalysts requires knowledge of the atomic scale coordination of the metal to the oxide support in various environmental conditions.

Pre-treatment of atomically dispersed metal catalysts produced *via* impregnation of metal salts typically starts with high temperature oxidation to remove ligands remaining from synthesis. For reducible oxide supports, this results in atomically dispersed metals localizing at cation vacancies at the oxide surface.[8–10] Catalysts are often then reduced to decrease the oxygen coordination number to the atomically dispersed metal and enable interaction with reactants or adsorbing molecules. If the reducing agent is CO, oxygen is removed as CO_2, after which CO can bond to the atomically dispersed metal site.[11–13] CO is known to impart mobility to atomically dispersed metal species, allowing species to adopt different coordination sites on the support.[13,14] Alternatively, when materials are reduced in hydrogen, oxygen is removed *via* the formation of water and new hydroxyl groups form, which can modify atomically dispersed metal site characteristics.[15–18]

Here we clarify how the local environment of atomically dispersed Rh species on anatase TiO_2 is influenced by varying reductive pre-treatments. We demonstrate that distinct local environments for Rh species result from reduction treatments under CO and H_2. We attribute differences to varying proximal hydroxyl characteristics, which modify CO desorption processes from Rh. Our findings highlight how subtle changes in local environment can modify the properties of atomically dispersed metals. These studies also highlight how characterizing atomically dispersed metal catalysts by temperature programmed desorption (TPD) of CO analysed by Fourier transform infrared (FTIR) spectroscopy, combined with density functional theory (DFT) calculations, is a powerful approach to elucidate metal coordination. It is important to note that agreement between experimental and DFT calculated IR frequencies of bound CO could not unequivocally assign the structure of the active site, and that the addition of TPD analysis and comparison to DFT calculated adsorption energies enabled the distinguishing of active site structures.[19]

To synthesize atomically dispersed Rh on TiO_2, we applied principles of strong electrostatic adsorption (SEA) to high

[a] *Department of Chemical Engineering, University of California Santa Barbara, Santa Barbara, California 93106, USA. E-mail: pchristopher@ucsb.edu*
[b] *Dipartimento di Scienza dei Materiali, Università di Milano-Bicocca, via Cozzi 55, 20125 Milano, Italy. E-mail: gianfranco.pacchioni@unimib.it*
[c] *The University of Da-Nang, University of Science and Technology, 54 Nguyen Luong Bang, Da-Nang 550000, Vietnam*

† Electronic supplementary information (ESI) available: Experimental methods; synthesis, probe CO FTIR, TPD and Redhead analysis. Computational methods and models; DFT, single Rh atom on TiO_2 (101) and stepped TiO_2 (145) surfaces, adsorption of a single CO molecule, adsorption of two CO molecules, and metallic Rh cluster on TiO_2 (101). See DOI: 10.1039/d0cy00146e

‡ These authors contributed equally to this work.

surface area (290 m^2 g^{-1}) 5 nm diameter anatase TiO_2 particles with low Rh weight loadings (0.1%).[5] Catalysts were *ex situ* and *in situ* pre-treated at 350 °C in O_2, which rendered Rh species unable to adsorb CO following room temperature exposure, see Fig. S1,† suggesting Rh species resided in cation (Ti) vacancies in the lattice.[9] The influence of reductive treatments on Rh local coordination was investigated using CO probe molecule FTIR-TPD following pre-treatment of the sample in H_2 at 100–300 °C or in CO at 300 °C. The CO reduction temperature of 300 °C was chosen because no significant CO adsorption was observed following 1 hour reduction at lower temperature.[9]

When the material was pre-treated in CO at 300 °C or in H_2 at 100 °C, and then exposed to 10% CO in argon at room temperature, bands at ~2092–2094 and ~2029–2031 cm^{-1} were observed in room temperature FTIR measurements (see Fig. 1 and Table 1). These bands are assigned to the symmetric and asymmetric stretches of CO ligands in oxide supported Rh gem-dicarbonyl species, $Rh(CO)_2$, unique to atomically dispersed Rh.[20]

The ability of Rh to adsorb CO in the $Rh(CO)_2$ structure following reductive treatments is evidence that reduction drove Rh to move from a cation replaced coordination to a supported coordination environment, as we observed previously for Rh on rutile TiO_2.[9] Extensive DFT+U calculations of atomic Rh on anatase TiO_2 (see ESI,† Fig. S2–S5 and Tables S1 and S2) support this assignment: a model of $Rh(CO)_2$ consisting of a Rh adsorbed on anatase (101) and interacting with two lattice O_{2c} (Fig. S6a†) result in computed (scaled) frequencies at 2097 and 2026 cm^{-1} for the complex formed on the terrace sites, and of 2095 and 2031 cm^{-1} for $Rh(CO)_2$ formed at anatase (145) step sites (Table S2†). The lack of CO bands in the experimental FTIR spectra at frequencies characteristic of linear (~2080–2040 cm^{-1}) and bridge (~1950–1850 cm^{-1}) bound CO on Rh clusters confirms that Rh primarily existed as atomically dispersed species following CO exposure.[21]

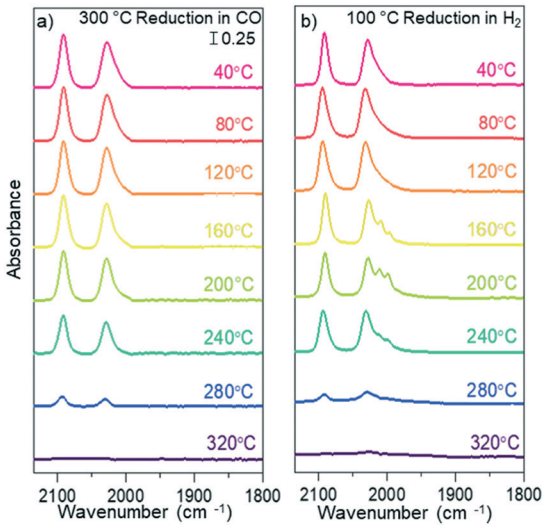

Fig. 1 FTIR spectra following CO saturation and during a TPD of CO from $Rh(CO)_2$ supported on anatase TiO_2 following varied pre-treatment conditions: a) reduction in CO at 300 °C and b) reduction in H_2 at 100 °C.

The CO stretching frequencies and full width at half maxima (FWHM) of the $Rh(CO)_2$ bands were similar for both pre-treatments (~10–15 cm^{-1}), see Table 1. The observed CO stretch FWHMs, which characterize the homogeneity of the local coordination environment of $Rh(CO)_2$ species, are smaller than typically observed for $Ir(CO)_2$ and $Rh(CO)_2$ species on oxide supports (>15 cm^{-1}), but broader than observed for zeolite supports (<10 cm^{-1}).[7,22,23] The narrowness of the CO stretches in comparison to previous observations on oxide supports and the similarities between the two pre-treatments suggest that the $Rh(CO)_2$ species sit in relatively homogeneous coordination environments on the support.

While the $Rh(CO)_2$ IR spectra for the CO and H_2 pre-treated samples appear indistinguishable at room temperature, significant differences were observed during TPD experiments. For the CO pre-treated sample, the maximum rate of CO desorption occurred at 240 °C, with the simultaneous loss of the symmetric and asymmetric stretching features, see Fig. 1a and S7.† The concurrent loss of both bands suggests both CO molecules have similar binding energy to Rh and desorb simultaneously. This is consistent with the DFT calculations: the 2 CO molecules have binding energies of 2.03 eV and 2.05 eV for the terrace $Rh(CO)_2$ complex, and of 1.96 eV and 2.0 eV for the step $Rh(CO)_2$ complex, Table S2† (computed values are about 0.5 eV larger than the measured E_{ads} from TPD spectra, Table 1). Further, the relatively narrow temperature window of desorption, in comparison to CO desorption from metal clusters, supports the uniformity in coordination environment of the Rh species, an aspect which is corroborated by the similar properties computed at DFT level for $Rh(CO)_2$ species formed on terrace or step sites.[3,6] When the sample was pre-treated in H_2 at 100 °C, additional CO stretching features at 2012 and 1999 cm^{-1} became apparent at 120 °C during the TPD. This indicates that the $Rh(CO)_2$ coordination environments are distinct following CO and H_2 pre-treatments. Importantly, this would not have been concluded by looking at the static IR spectra at room temperature, which is a commonly used approach.[22–28]

To understand the origin of the features at 2012 and 1999 cm^{-1}, spectra collected during the CO TPD following 100 °C pre-treatment in H_2 were deconvoluted into 4 distinct bands, (see Fig. 2a and Table 1). The rate of change of peak areas, and thus change in surface adsorbate concentration, was analysed as a function of temperature, see Fig. 2b. This analysis identifies that the maximum rate of formation of the bands at 2012 and 1999 cm^{-1} occurs simultaneously with a maxima in the rate of loss of $Rh(CO)_2$ species at 160 °C. See the ESI† for discussion on peak deconvolution and integration during the TPD. This provides evidence that for some $Rh(CO)_2$ species on the sample reduced at 100 °C in H_2, an intermediate species is formed during CO desorption, rather than both CO molecules desorbing simultaneously.

Table 1 Experimentally observed CO stretching frequencies ω (cm^{-1}), corresponding full width at half maximum (FWHM), and adsorption energy E_{ads} (eV) calculated using Redhead analysis[29–31]

	ω_1 (cm^{-1})	ω_2 (cm^{-1})	$FWHM_1$	$FWHM_2$	$\sim E_{ads}$ (eV)
300 °C CO reduced $Rh(CO)_2$	2092	2029	11.5	15.2	1.5
100 °C H_2 reduced [a]$Rh(CO)_2$	2094	2031	13.2	13.8	1.3
[b]$Rh(CO)_2$	2094	2031	13.2	13.8	1.5
[c]Rh(CO)	2012, 1999		12.9, 8.0		1.7

[a] First desorption event associated with loss of intensity in $Rh(CO)_2$. [b] Second desorption event associated with loss of intensity in $Rh(CO)_2$. [c] Desorption event associated with loss of intensity of species formed during TPD.

The remaining intensity of the $Rh(CO)_2$ bands showed a second maxima in the rate of loss at 240 °C, similar to what was observed for the $Rh(CO)_2$ species following 300 °C CO pretreatment. This suggests that some fraction of the $Rh(CO)_2$ formed following H_2 reduction are consistent with those observed following CO reduction. The maximum rate of loss of the peaks at 2012 and 1999 cm^{-1} was observed at ~240–300 °C, as shown in Fig. 2b. Thus, the intermediate species formed during the TPD for the material reduced at 100 °C in H_2 exhibits a stronger CO binding energy as compared to the $Rh(CO)_2$ species that was common to both pretreatments.[32,33]

Based on known differences in H_2 and CO reductions, and the unfavourable energy associated with oxygen vacancy formation on the anatase surface, hydroxyl interactions with $Rh(CO)_2$ is the most favourable hypothesis to explain the difference between species formed in the two treatments. Increasing the H_2 reduction temperature led to an increase in the hydroxyl density and diversity on the TiO_2 surface, as observed from changes to the hydroxyl region of the FTIR spectra, 3000–4000 cm^{-1} (Fig. S8a†).[34–37] Furthermore, adsorbed water indicated by features at ~1260 and 1100 cm^{-1} was observed after H_2 reduction, but not CO reduction, demonstrating an increased oxide surface complexity (Fig. S8b†).[34–36,38] Increased hydroxyl coverage on the TiO_2 surface caused by increased reduction temperature in H_2 increased the heterogeneity of the local coordination environment of $Rh(CO)_2$ species. The increased heterogeneity in Rh local coordination environment following reduction at 200 °C in H_2, compared to 100 °C, is evidenced by broadening of the $Rh(CO)_2$ asymmetric band FWHM (24.0 cm^{-1}), as well as CO bands at 1999–2012 cm^{-1} associated with intermediate species formed during the TPD. When the same material was reduced in H_2 at 300 °C, Rh clusters formed, demonstrated by the emergence of a CO vibrational stretch between the $Rh(CO)_2$ symmetric and asymmetric stretches, which is characteristic of linear bound CO on small clusters of Rh (~2050 cm^{-1}). However, a significant quantity of $Rh(CO)_2$ species were still observed, although with modified CO TPD characteristics likely due to changes in local coordination from support hydroxylation (Fig. S9†).

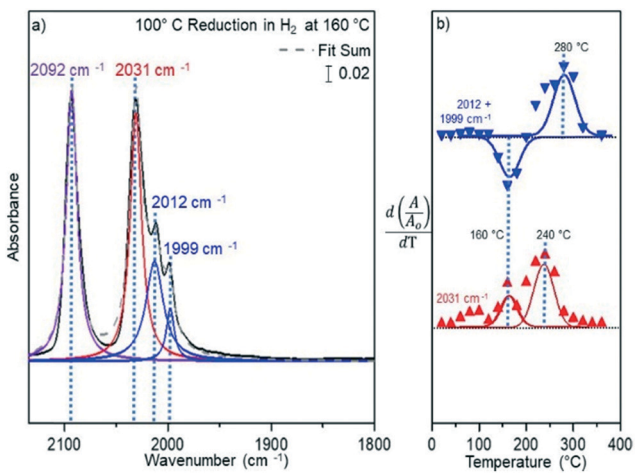

Fig. 2 a) CO probe molecule FTIR spectra of sample reduced in H_2 at 100 °C taken during CO TPD at 160 °C. Peaks were deconvoluted from the original spectra in black, with the $Rh(CO)_2$ symmetric stretch at 2092 cm^{-1} in purple, the $Rh(CO)_2$ asymmetric stretch at 2031 cm^{-1} in red, and bands formed at 2012 and 1999 cm^{-1} in blue. b) Comparison of temperature dependent rate of change in normalized CO band intensity (A/A_0) for the asymmetric stretch (2031 cm^{-1}, red) and newly formed features (2012 and 1999 cm^{-1}, blue). Maxima and minima in the rate of change, associated with the formation and loss of species, are highlighted at characteristic temperatures.

In order to identify the nature of the different Rh species, including the experimentally hypothesized $Rh(OH)(CO)_2$, an extensive series of models of Rh atomic species and their computed properties was considered by DFT calculations (see ESI†). Two modelled configurations matched experimental observations; Fig. 3a where the Rh atom bounds to two lattice O_{2c} ions of the surface, $Rh(CO)_2$, and Fig. 3b that differs only by the presence of an additional neighboring surface OH group, $Rh(OH)(CO)_2$. Surprisingly, the two complexes exhibit similar CO vibrational features: on terrace sites 2097 and 2026 cm^{-1} for $Rh(CO)_2$, and 2090 and 2019 cm^{-1} for $Rh(OH)(CO)_2$; on step sites 2095 and 2031 cm^{-1} for $Rh(CO)_2$, and 2096 and 2029 cm^{-1} for $Rh(OH)(CO)_2$, Table S2.† Clearly, a distinction of the two species based on the vibrational properties of the $Rh(CO)_2$ complex is not possible. However, while $Rh(CO)_2$ gives rise to a simultaneous desorption of the CO molecules (E_{ads} about 2 eV), for $Rh(OH)(CO)_2$ the two CO molecules have distinct adsorption energies, hence desorption temperatures, with a CO molecule bound by 1.62 eV and the other by 2.72 eV. While the absolute DFT values of E_{ads} are systematically overestimated compared to experiment, the trend is correct, Table 1.

CO desorption leaves a Rh(OH)(CO) mono-carbonyl complex on the surface with a CO stretching frequency of

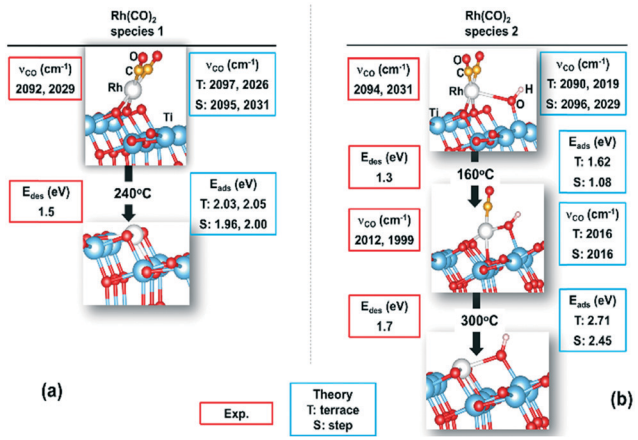

Fig. 3 Structure of $Rh(CO)_2$ species identified by FTIR-TPD spectra and DFT calculations and evolution with temperature on (a) (Rh)ads and (b) (RhOH)ads species. Red boxes (left): Experimental results; blue boxes (right): DFT results.

2016 cm^{-1} for both complexes formed on terraces or steps. This agrees with the IR features at 2012–1999 cm^{-1} observed experimentally, when no other species considered exhibits a stretching frequency in this region (see ESI†). CO binds to Rh(OH) with E_{ads} = 2.70 eV (terrace) or 2.90 eV (step), consistent with a higher CO desorption temperature for this species observed from experiments. It is hypothesized that the 2 distinct bands at 2012 and 1999 cm^{-1} observed in Fig. 2a arise from small differences in the adsorption site of Rh(OH)(CO) species, for example at terrace, step or kink sites on TiO_2. The agreement in CO vibrational frequencies and trend in CO desorption energy when comparing $Rh(CO)_2$, $Rh(OH)(CO)_2$ and Rh(OH)(CO) in the DFT calculations and experimental measurements provide strong evidence of the influence of reductant composition on Rh local coordination.

In summary, it was identified that when atomically dispersed Rh on anatase TiO_2 was reduced at 100 °C in H_2 or in 300 °C in CO, adsorbed CO had similar characteristics in static IR measurements at room temperature. However, based on TPD measurements compared with DFT calculations we propose for both pre-treatments $Rh(CO)_2$ species with two bonds to two lattice O atoms form, while in the case of H_2 pre-treatment an additional species with a proximal hydroxyl forms, $Rh(OH)(CO)_2$. This demonstrates how subtle changes in the local coordination of atomically dispersed metals can have strong influences on their surface chemistry.

Conflicts of interest

There are no conflicts to declare.

Acknowledgements

Work by GP and HVT was supported by the Italian MIUR through PRIN Project 20179337R7 MULTI-e "Multielectron transfer for the conversion of small molecules: an enabling technology for the chemical use of renewable energy" and grant Dipartimenti di Eccellenza – 2017 "Materials for Energy". Work by CA and PC was supported by Science Foundation (NSF) GOALI Grant CBET-1804128 and Mellichamp Initiative for Sustainability at University of California, Santa Barbara.

References

1 L. Liu and A. Corma, *Chem. Rev.*, 2018, **118**, 4981–5079.
2 J. C. Matsubu, S. Zhang, L. Derita, N. S. Marinkovic, J. G. Chen, G. W. Graham, X. Pan and P. Christopher, *Nat. Chem.*, 2017, **9**, 120–127.
3 H. V. Thang, G. Pacchioni, L. Derita and P. Christopher, *J. Catal.*, 2018, **367**, 104–114.
4 T. Y. Chang, Y. Tanaka, R. Ishikawa, K. Toyoura, K. Matsunaga, Y. Ikuhara and N. Shibata, *Nano Lett.*, 2013, **14**, 134–138.
5 L. Derita, S. Dai, K. Lopez-Zepeda, N. Pham, G. W. Graham, X. Pan and P. Christopher, *J. Am. Chem. Soc.*, 2017, **139**, 14150–14165.
6 L. Derita, J. Resasco, S. Dai, A. Boubnov, H. V. Thang, A. S. Hoffman, I. Ro, G. W. Graham, S. R. Bare, G. Pacchioni, X. Pan and P. Christopher, *Nat. Mater.*, 2019, **18**, 746–751.
7 A. S. Hoffman, C. Y. Fang and B. C. Gates, *J. Phys. Chem. Lett.*, 2016, **7**, 3854–3860.
8 X. A. D. Mayernick and M. J. Janik, *J. Catal.*, 2011, **278**, 16–25.
9 Y. Tang, C. Asokan, M. Xu, G. W. Graham, X. Pan, P. Christopher, J. Li and P. Sautet, *Nat. Commun.*, 2019, **10**, 4488.
10 B. Qiao, A. Wang, X. Yang, L. F. Allard, Z. Jiang, Y. Cui, J. Liu, J. Li and T. Zhang, *Nat. Chem.*, 2011, **3**, 634–641.
11 R. R. Cavanagh and J. T. Yates, *J. Chem. Phys.*, 1981, **74**, 4150.
12 J. T. Yates, T. M. Duncan, S. D. Worley and R. W. Vaughan, *J. Chem. Phys.*, 1979, **70**, 1219.
13 K. I. Hadjiivanov and G. N. Vayssilov, *Adv. Catal.*, 2002, **47**, 307–511.
14 B. R. Goldsmith, E. D. Sanderson, R. Ouyang and W. X. Li, *J. Phys. Chem. C*, 2014, **118**, 9588–9597.
15 G. S. Parkinson, Z. Novotny, G. Argentero, M. Schmid, J. Pavelec, R. Kosak, P. Blaha and U. Diebold, *Nat. Mater.*, 2013, **12**, 724–724.
16 K. Hadjiivanov, *Adv. Catal.*, 2014, **57**, 99–318.
17 G. D. Panagiotou, T. Petsi, K. Bourikas, C. S. Garoufalis, A. Tsevis, N. Spanos, C. Kordulis and A. Lycourghiotis, *Adv. Colloid Interface Sci.*, 2008, **142**, 20–42.
18 P. B. Panayotov and J. T. Yates, *J. Am. Chem. Soc.*, 1988, **110**, 2074–2081.
19 H. A. Aleksandrov, K. M. Neyman, K. I. Hadjiivanov and G. N. Vayssilov, *Phys. Chem. Chem. Phys.*, 2016, **18**(32), 22108–22121.
20 C. W. Garland and A. Yang, *J. Phys. Chem.*, 1957, **69**, 1504–1512.
21 A. K. Smith, F. Hugues, A. Theolier, J. M. Basset, R. Ugo, G. M. Zanderighi, J. L. Bilhou and W. F. Graydon, *Inorg. Chem.*, 1979, **18**, 3104–3112.

22 P. Serna and B. C. Gates, *J. Am. Chem. Soc.*, 2011, **133**, 4714–4717.
23 J. C. Matsubu, V. N. Yang and P. Christopher, *J. Am. Chem. Soc.*, 2015, **137**, 3076–3084.
24 J. T. Yates and K. Kolasinski, *J. Chem. Phys.*, 1983, **79**, 1026.
25 E. Ivanova, M. Mihaylov, F. Thibault-Starzyk, M. Daturi and K. Hadjiivanov, *J. Mol. Catal. A: Chem.*, 2007, **274**, 179–184.
26 F. Zaera, *Chem. Soc. Rev.*, 2014, **43**, 7624–7663.
27 E. Varga, P. Pusztai, L. Ovari, A. Oszko, A. Erdohelyi, C. Papp, H. P. Steinruck, Z. Konya and J. Kiss, *Phys. Chem. Chem. Phys.*, 2015, **17**, 27154–27166.
28 S. Trautmann and M. Baerns, *J. Catal.*, 1994, **150**, 335–344.
29 P. A. Redhead, *Vacuum*, 1962, **12**, 203–211.
30 V. Nehasil, I. Star and V. Matoln, *Surf. Sci.*, 1995, **152**, 105–109.
31 P. A. Thiel, E. D. Williams, J. T. Yates and W. H. Weinberg, *Surf. Sci.*, 1979, **84**, 54–64.
32 H. Cheng and A. Selloni, *Phys. Rev. B: Condens. Matter Mater. Phys.*, 2009, **79**, 2–5.
33 Y. He, O. Dulub, H. Cheng, A. Selloni and U. Diebold, *Phys. Rev. Lett.*, 2009, **120**, 106105.
34 K. I. Hadjiivanov and D. G. Klissurski, *Chem. Soc. Rev.*, 1996, **25**, 61–69.
35 T. Bezrodna, G. Puchkovska, V. Shymanovska, J. Baran and H. Ratajczak, *J. Mol. Struct.*, 2004, **700**, 175–181.
36 D. A. Panayotov and J. T. Yates, *Chem. Phys. Lett.*, 2005, **410**, 11–17.
37 G. Li, L. Li, J. Boerio-Goates and B. F. Woodfield, *J. Am. Chem. Soc.*, 2005, **127**, 8659–8666.
38 P. Basu, D. Panayotov and J. T. Yates, *J. Am. Chem. Soc.*, 1988, **110**, 2074–2081.